

Figure S1: Sequential recruitment of ER coactivators to different ER binding sites, related to Figure 1 (a) *GREB1* distal enhancer ER binding site (b) *GREB1* proximal promoter ERE1 site (c) *TFF1* distal enhancer ER binding site. Shown are ChIP experiments in MCF-7 cells treated with 100 nM E2 for indicated time periods. Data are represented as mean  $\pm$  SEM.

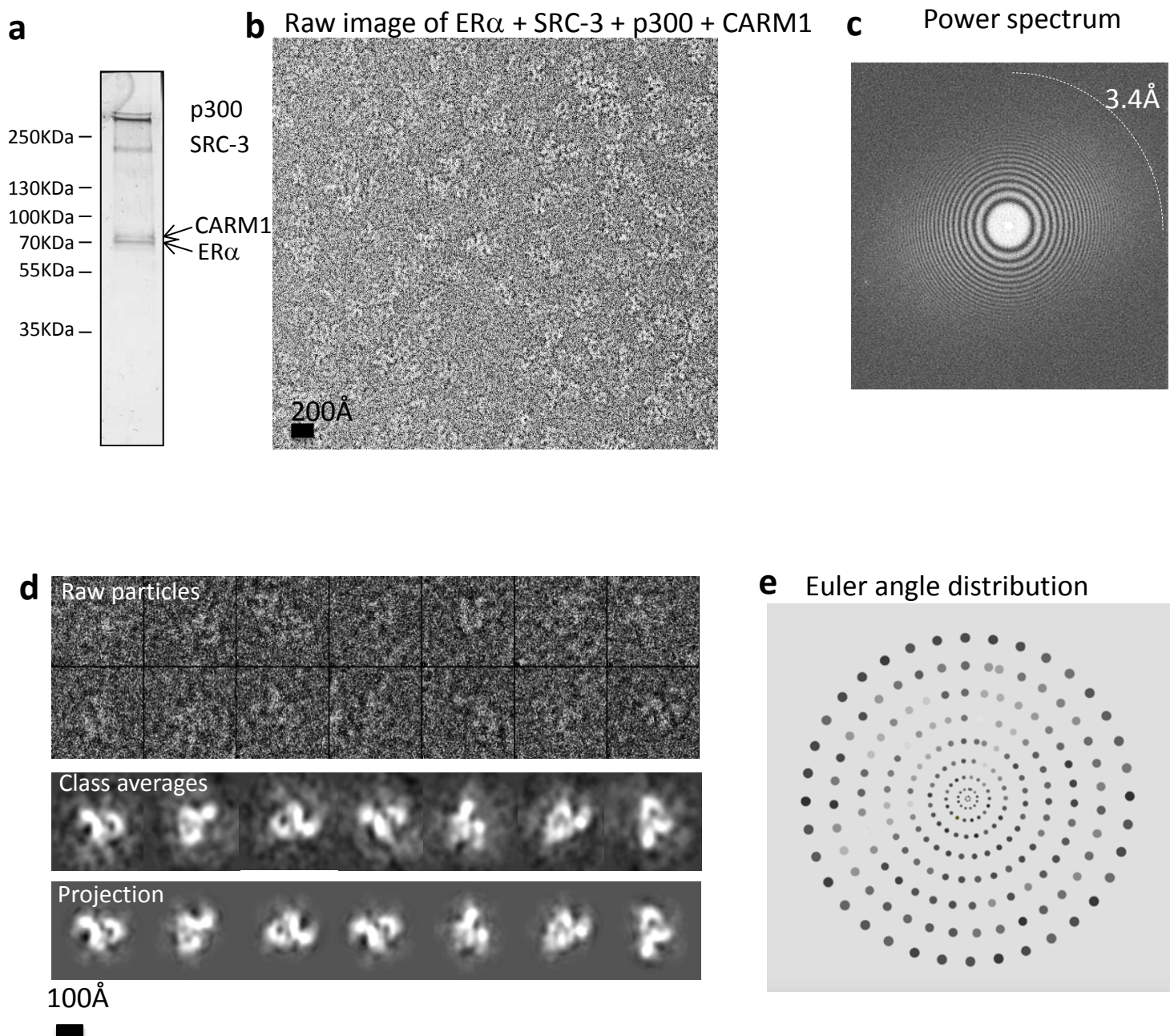
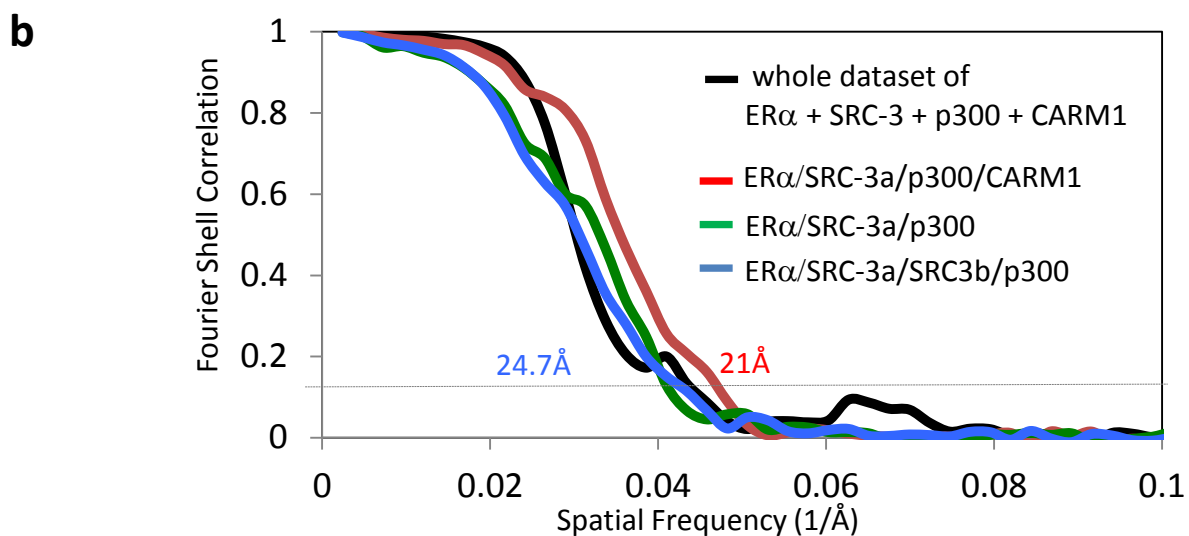
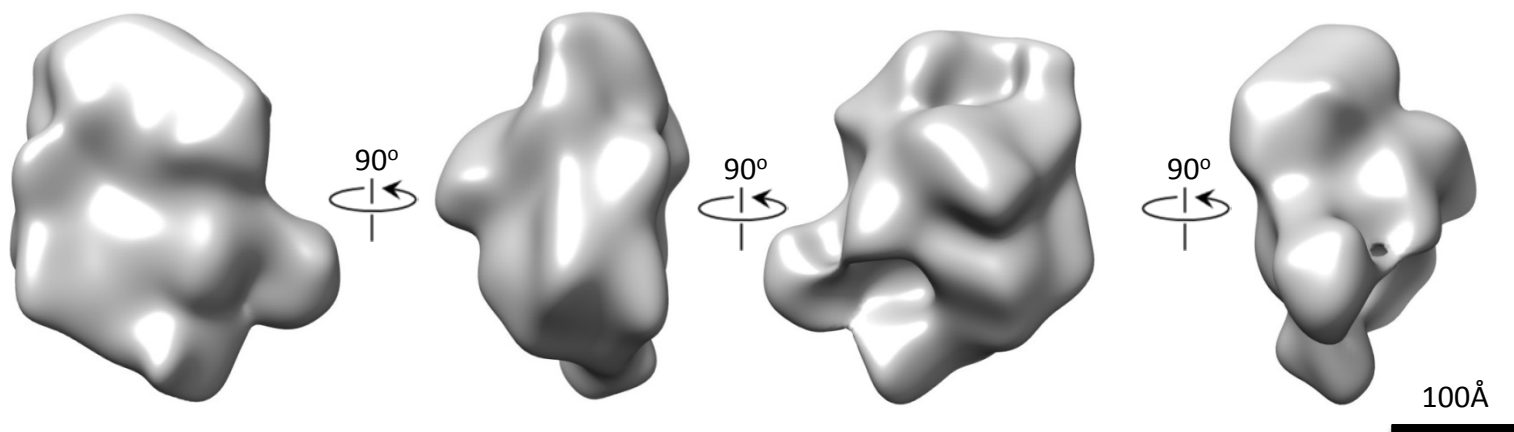


Figure S2: Raw images and class averages of the ERE/ER/SRC-3/p300/CARM1 complex, related to Figure 2 and STAR Methods (a) Silver stain of a SDS-PAGE gel with the assembled complex (b) raw images (c) Power spectra of the images (d) Raw particles, class averages and 3D projection of the images (e) Euler angle distribution of the particles.

**a** Starting model of ER $\alpha$  + SRC-3 + p300 + CARM1 dataset



**c** Tilt pair validation of ER $\alpha$  + SRC-3 + p300 + CARM1

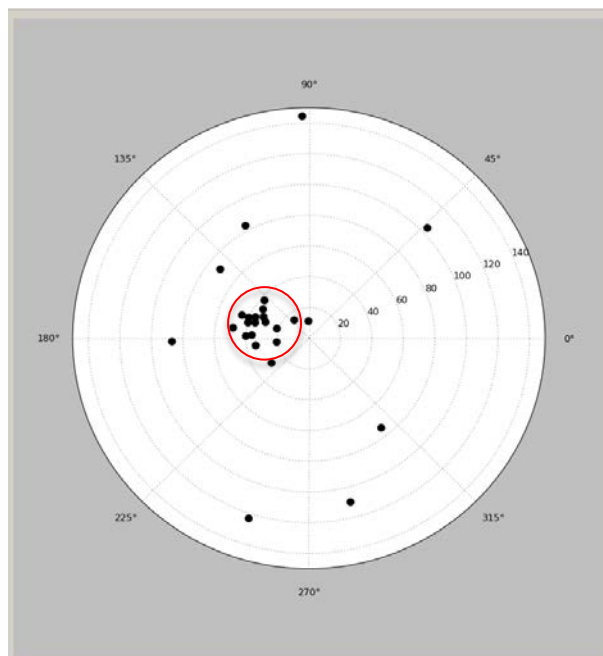
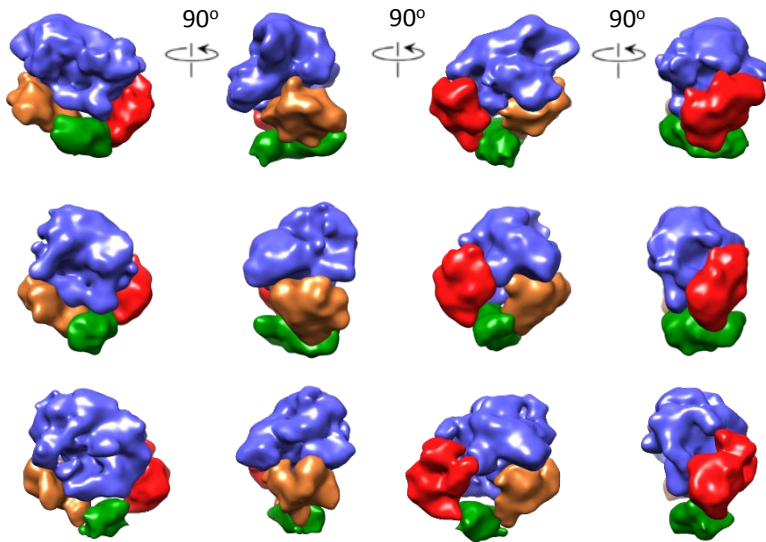
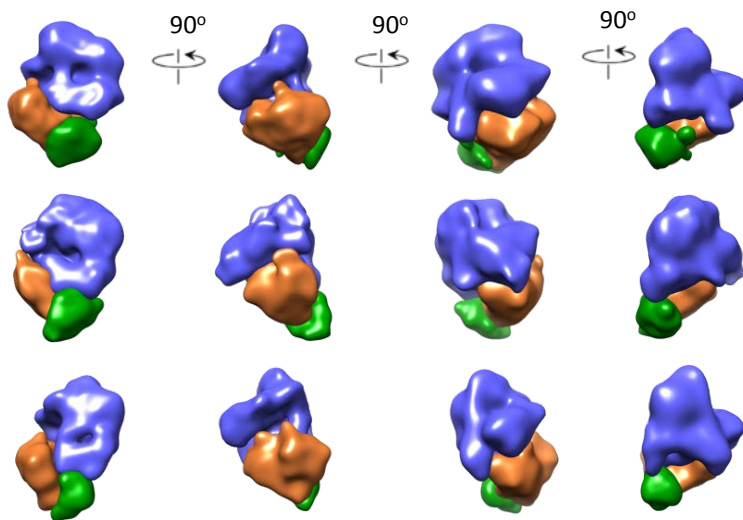


Figure S3, related to STAR Methods: (a) A starting model of the ERE/ER/SRC-3/p300 complex (b) Gold standard FSC curve of the structures for refinement of whole dataset and subsets of each complex. (c) Tilt pair validation. The density map of the complex reconstructed using the RELION software.

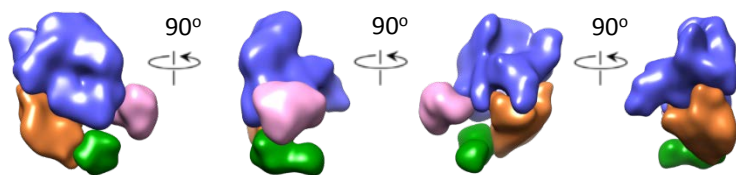
**a** ERE/ER $\alpha$ /SRC-3a/SRC-3b/p300 complex from three different datasets



**b** ERE/ER $\alpha$ /SRC-3a/p300 complex from three different datasets



**c** ERE/ER $\alpha$ /SRC-3a/p300/CARM1 complex from ER $\alpha$  + SRC-3 + p300 + CARM1 dataset (map 1C)



**d** ERE/ER $\alpha$ /SRC-3a/p300/CARM1/Fab complex from ER $\alpha$  + SRC-3 + p300 + CARM1 + Fab dataset (map 2E)

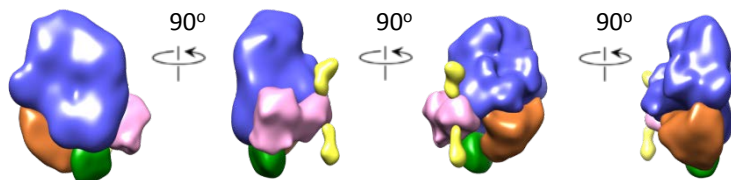


Figure S4: Identification of CARM1 location in the complex, related to Figure 2. (a) Segmentation of ERE/ER $\alpha$ /SRC-3a/SRC-3b/p300 complex from three different datasets (from top to bottom). The complex from ER $\alpha$  + SRC-3 + p300 + CARM1 dataset (top). The complex from ER $\alpha$  + SRC-3 + p300 + CARM1 + Fab dataset (middle). The complex from previous published dataset (EMDBID:EMDB-6259) ER $\alpha$  + SRC-3 + p300 (bottom). (b) Segmentation of ERE/ER $\alpha$ /SRC-3a/p300 complex from three different datasets (from top to bottom). The complex from ER $\alpha$  + SRC-3 + p300 + CARM1 dataset (top). The complex from ER $\alpha$  + SRC-3 + p300 + CARM1 + Fab dataset (middle). The complex from previous published dataset (EMDBID:EMDB-6259) ER $\alpha$  + SRC-3 + p300 (bottom). (c) Segmentation of ERE/ER $\alpha$ /SRC-3a/p300/CARM1 complex from ER $\alpha$  + SRC-3 + p300 + CARM1 dataset. (d) Segmentation of ERE/ER $\alpha$ /SRC-3a/p300/CARM1 complex with Fab from ER $\alpha$  + SRC-3 + p300 + CARM1 + Fab dataset.

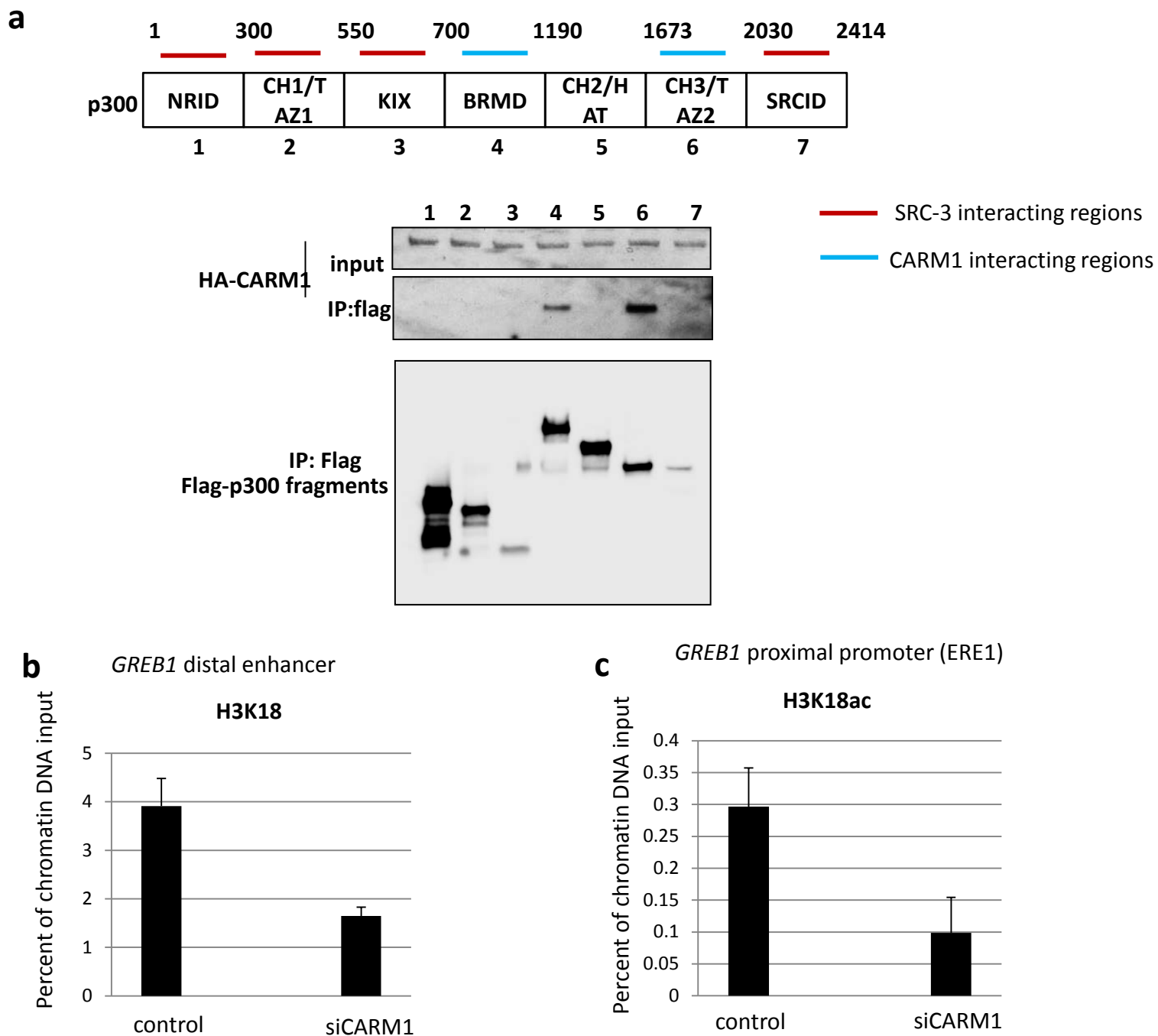


Figure S5, related to Figure 4: (a) SRC-3 and CARM1 contact different regions in p300. Shown is a co-IP experiment in cells transiently transfected with HA-CARM1 and different flag tagged p300 fragments. The red lines represent p300 regions interacting with SRC-3 and the blue lines represent p300 regions interacting with CARM1. (b-c) The levels of H3 K18 acetylation decreased upon CARM1 knockdown at *GREB1* distal enhancer ER binding site (b) and *GREB1* proximal promoter ERE1 site (c). Shown are ChIP experiments using H3 K18 acetylation antibody in MCF-7 cells stimulated with 100 nM E2 for 30 minutes.